SI

Phase transition and Ionic conduction enhancement induced by co-doping LiI and MnI_2 in one-dimensional lead iodide perovskite

Ya-Ru Kong,[a] Wei Qiu,[b] Guo-Qin Zhang,[a] Dong-sheng Shao,[a] Zheng-Fang Tian,[b] Hong-Bin Luo,*[a] Xue-Wei Pan,[a] Jin Zhang,[a] Xiao-Ming Ren*[a, c, d]

[a] State Key Laboratory of Materials-Oriented Chemical Engineering and College of Chemistry and Molecular Engineering, Nanjing Tech University, Nanjing 211816, P. R. China

[b] Hubei Key Laboratory for Processing and Application of Catalytic Materials, Huanggang Normal University, Huanggang 438000, P. R. China

[c] College of Materials Science and Engineering, Nanjing Tech University, Nanjing 211816, P. R. China

[d] State Key Laboratory of Coordination Chemistry, Nanjing University, Nanjing 210093, P. R. China

Tel: 86-25-58139476

E-mail: hbluo@ njtech.edu.cn (HBL); xmren@njtech.edu.cn (XMR)

Content

Experimental section

Chemicals and Materials

All of chemicals and solvents were purchased from commercial suppliers and used without further purification. $[Bu_4N]PbI_3$ (Bu_4N^+ = tetrabutylammonium) was prepared following the procedure in literature.[1]

Preparation of co-doped Mn^{2+} and Li^+ samples

The co-doped samples $Bu_4N_{1-x}Li_xMn_xPb_{1-x}I_3$ were mechanochemically prepared using a similar procedure. The *x* value was determined by ICP technique, and the five hybrids are labeled as $Bu_4N_{1-x}Li_xMn_xPb_{1-x}I_3$ (x = 0, 0.011, 0.042, 0.11 and 0.14). Each sample was also characterized by EDS and microanalysis for C, H and N elements, and these results are summarized in Table S1.

Characterization

Elemental analyses (C, H, N) were performed with an Elementar Vario EL. Inductively coupled plasma-mass spectrometry (ICP-MS) analyses were performed by a PHI 5000 Versa Probe ICP spectrometer. EDS was carried out by means of a Hitachi S-3400N scanning electron microscope. Thermogravimetric (TG) measurements were performed with a SDT Q600 thermogravimetric analyzer in 300−1073 K under N_2 atmosphere, and the heating rate is 20 K min^{-1}. DSC measurements were performed on a NETZSCH DSC 204F1 Phoenix with a temperature change rate of 10 K min^{-1}. Raman spectra was conducted on a Thermo Fisher Scientific DXR2 instrument with a 532 nm laser light irradiation from 26–3500 cm^{-1}. Fourier transform infrared (FT-IR) spectrum was recorded on a Thermo Scientific Nicolet iS10 spectrophotometer in the regime of 4000–400 cm^{-1}. X-band EPR spectra were obtained using Bruker EMX Electron Spin Resonance system at ambient condition. X-ray photoelectron spectroscopy (XPS) equipped with a standard and monochromatic Al K_α X-ray source (Thermo Fisher Nexsa) operated at 72 W (12 kV, 6 mA) was employed for surface analysis, and the binding energies were referenced to the internal standard C 1s main peak at 285.0 eV.

Powder X-ray diffraction (PXRD) data were collected on a MiniFlex600 powder diffractometer at ambient temperature, and the measurement was operated at 40 kV and

40 mA, and using Cu Kα radiation (λ = 1.5404 Å). Temperature dependent PXRD patterns were recorded by Bruker D8 ADVANCE instrument equipped with an xrk900 sample cell.

Dielectric permittivity and impedance spectra were recorded by a concept 80 system (Novocontrol, Germany) in 273−373 K, and the frequencies span from 1 to 10^7 Hz. The chronoamperometry was recorded by a Gamry Reference 600+ electrochemical workstation in 318−373 K. All of samples were prepared in the form of a disk with the diameter of 7 mm and the thickness of ca.1.4 mm.

Table S1: Microanalysis for C, H and N elements and EDS for Pb and Mn elements in each hybrid

$Bu_4N_{1-x}Li_xMn_xPb_{1-x}I_3$	**Micro analysis/found(calc.)**			**EDS mapping results**		
	C / %	**H / %**	**N / %**	**Pb/at.%**	**Mn/at.%**	**Mn/Pb (found/calc.)**
x = 0	23.09 (23.14)	4.30 (4.37)	1.58 (1.69)	NA	NA	NA
x = 0.011	22.35 (23.01)	4.19 (4.34)	1.46 (1.68)	1.91	0.06	0.031 (0.010)
x = 0.042	22.00 (22.61)	4.05 (4.27)	1.48 (1.65)	4.22	0.21	0.049 (0.053)
x = 0.11	21.08 (21.71)	3.98 (4.10)	1.40 (1.58)	3.19	0.38	0.119 (0.11)
x = 0 .14	20.78 (21.32)	3.94 (4.03)	1.40 (1.55)	2.56	0.45	0.176 (0.17)

Table S2: XPS binding energies in each hybrid and references

Element	E_b / eV					Ref.
	x = 0	x = 0.011	x = 0.042	x = 0.11	x = 0.14	
Pb 4f	141.83($4f_{5/2}$) 136.27($4f_{7/2}$)	142.12($4f_{5/2}$) 137.21($4f_{7/2}$)	142.00($4f_{5/2}$) 137.11($4f_{7/2}$)	141.94($4f_{5/2}$) 137.02($4f_{7/2}$)	141.87($4f_{5/2}$) 137.05($4f_{7/2}$)	2
I 3d	629.08($3d_{3/2}$) 617.63($3d_{5/2}$)	629.40($3d_{3/2}$) 617.98($3d_{5/2}$)	629.30($3d_{3/2}$) 617.82($3d_{5/2}$)	629.29($3d_{3/2}$) 617.74($3d_{5/2}$)	629.17($3d_{3/2}$) 617.76($3d_{5/2}$)	2
N 1s	400.74	401.25	401.30	401.17	401.23	3
C 1s	283.99	284.32	284.20	284.13	284.83	4

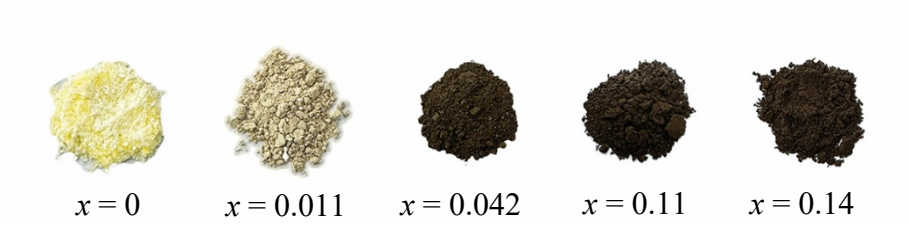

Fig. S1: Optical pictures of samples with x = 0–0.14.

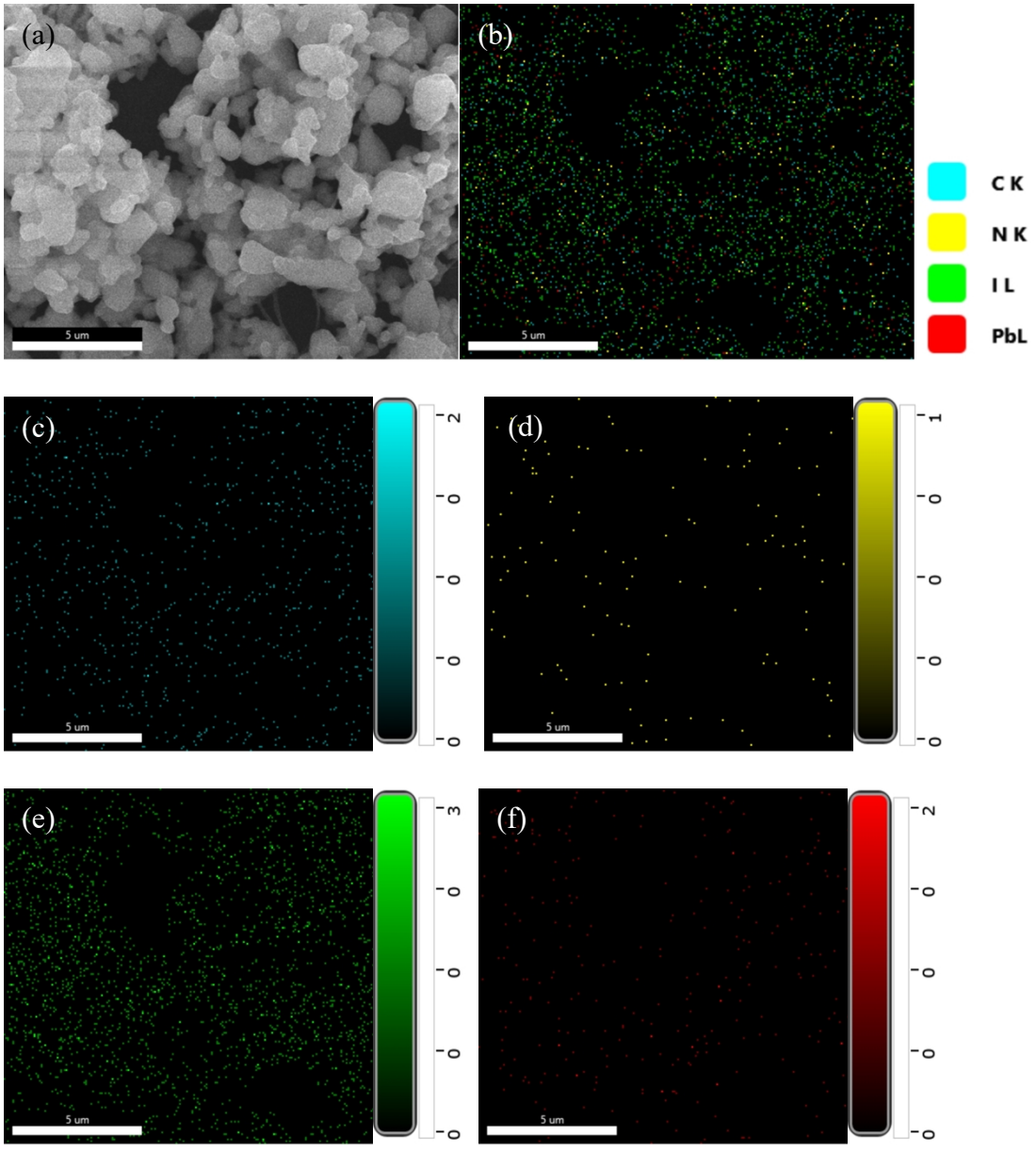

Fig. S2: SEM image and EDS of $Bu_4N_{1-x}Li_xMn_xPb_{1-x}I_3$ (x = 0). (a) Image, (b) element overlay, (c) C, (d) N, (e) I and (f) Pb elements.

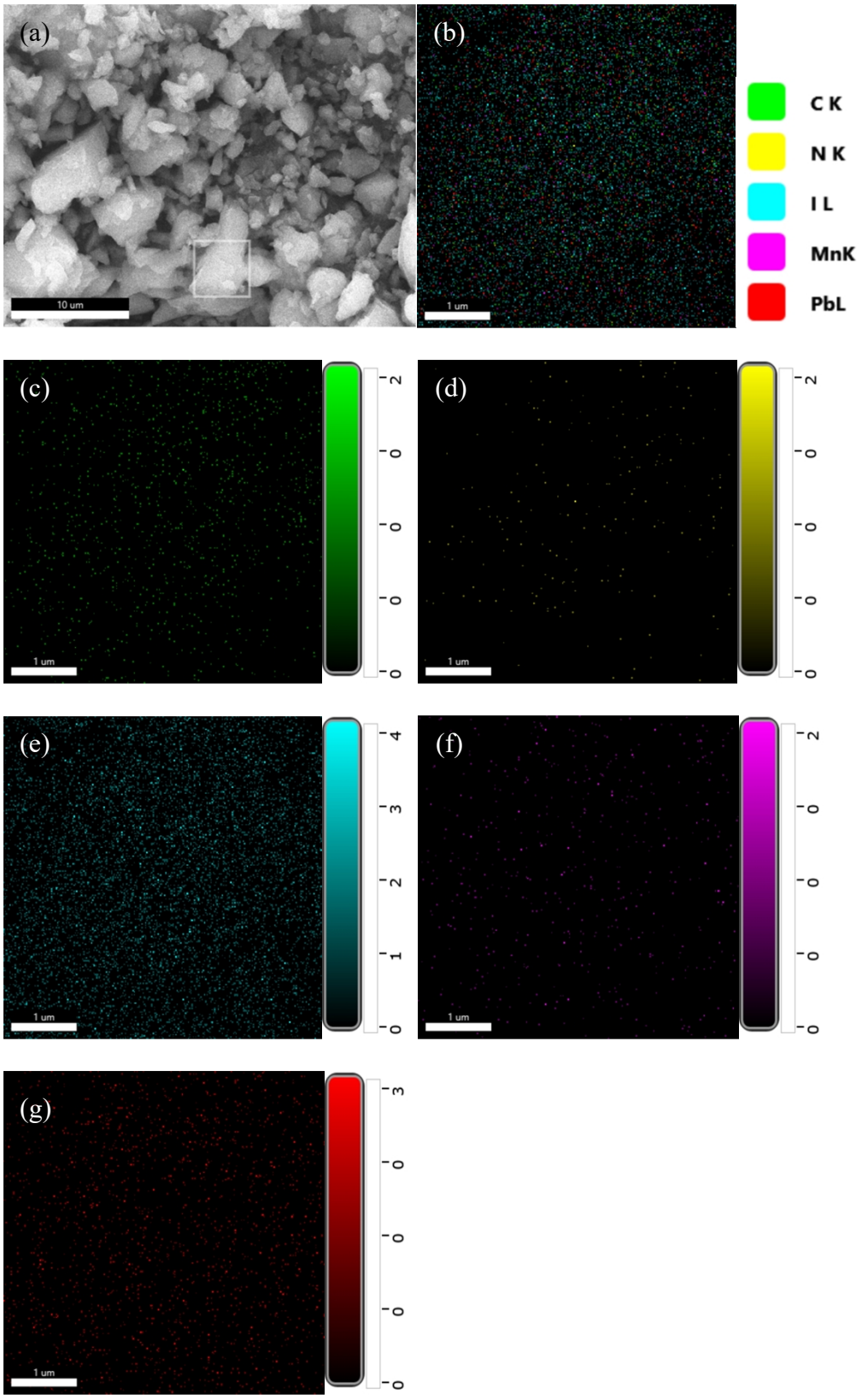

Fig. S3: SEM image and EDS of $Bu_4N_{1-x}Li_xMn_xPb_{1-x}I_3$ (x = 0.011). (a) Image, (b) element overlay, (c) C, (d) N, (e) I, (f) Mn and (g) Pb elements.

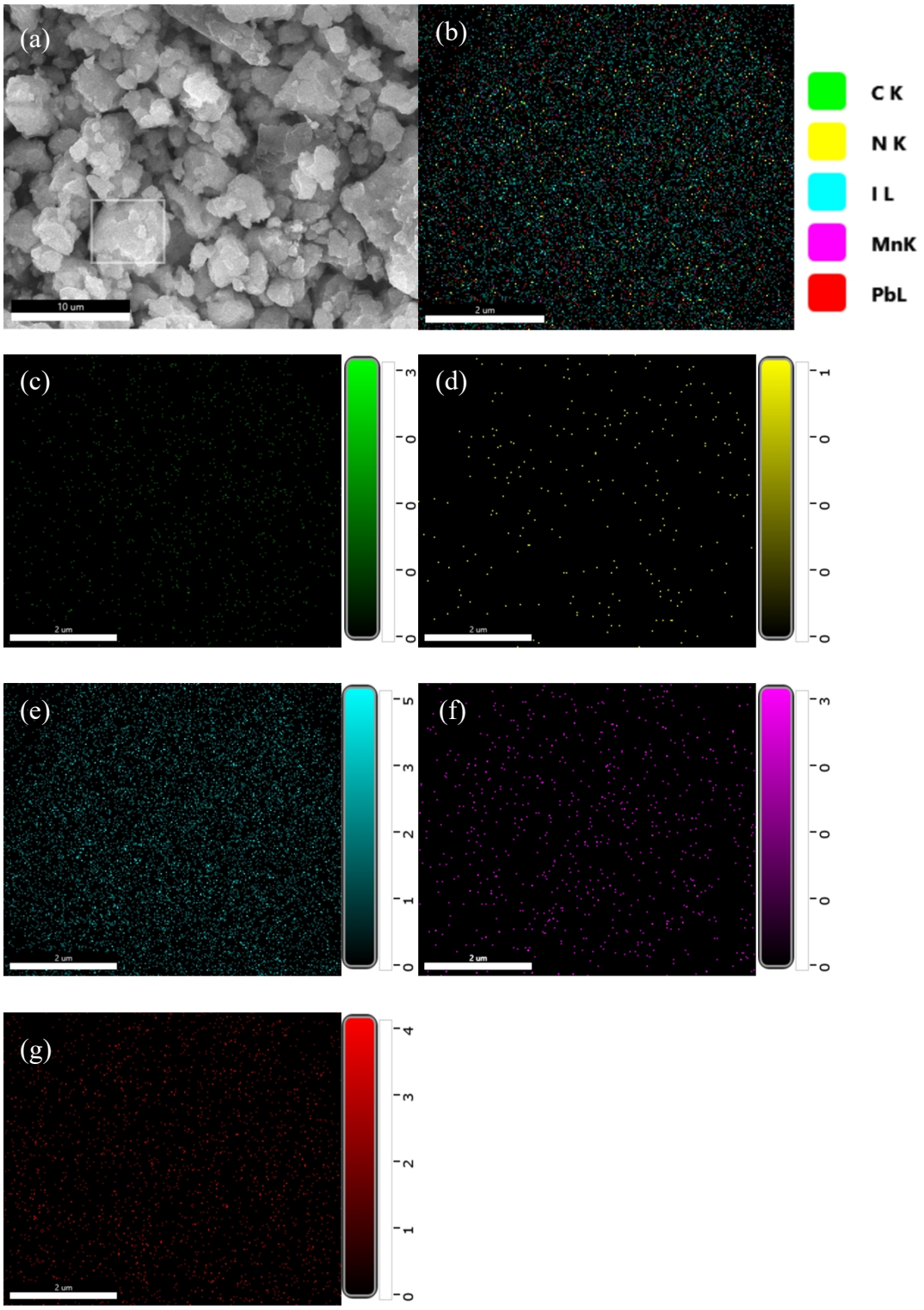

Fig. S4: SEM image and EDS of $Bu_4N_{1-x}Li_xMn_xPb_{1-x}I_3$ (x = 0.042). (a) Image, (b) element overlay, (c) C, (d) N, (e) I, (f) Mn and (g) Pb elements.

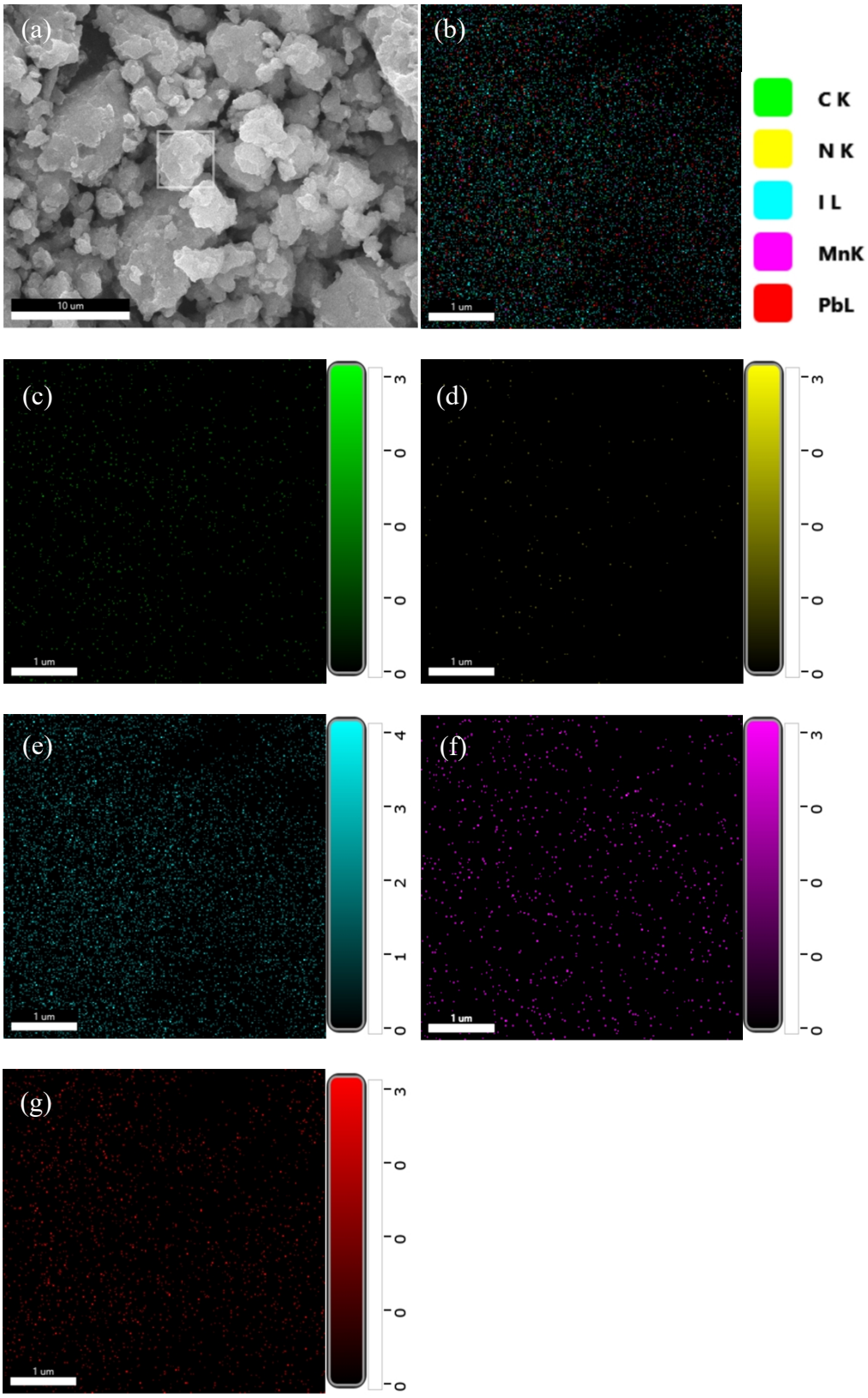

Fig. S5: SEM image and EDS of Bu_4N_{1-x} $Li_xMn_xPb_{1-x}I_3$ (x = 0.11). (a) Image, (b) element overlay, (c) C, (d) N, (e) I, (f) Mn and (g) Pb elements.

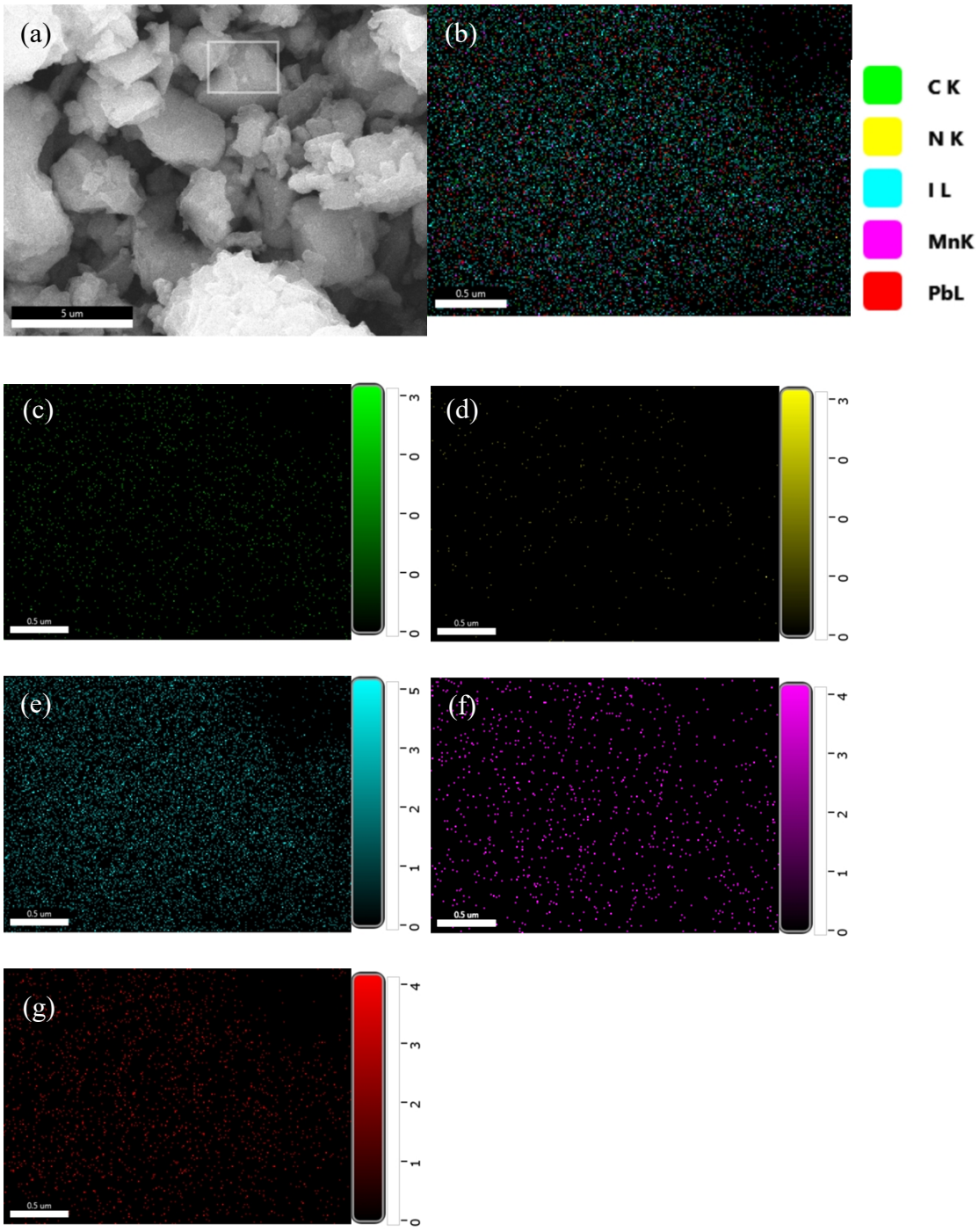

Fig. S6: SEM image and EDS of $Bu_4N_{1-x}Li_xMn_xPb_{1-x}I_3$ ($x = 0.14$). (a) Image, (b) element overlay, (c) C, (d) N, (e) I, (f) Mn and (g) Pb elements.

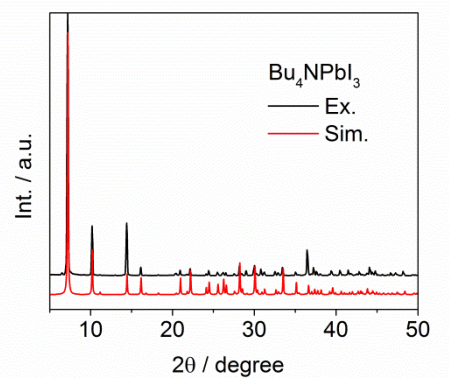

Fig. S7: Experimental and simulated PXRD patterns of $[Bu_4N]PbI_3$, and the simulated PXRD pattern was obtained from single crystal diffraction data of $[Bu_4N]PbI_3$.

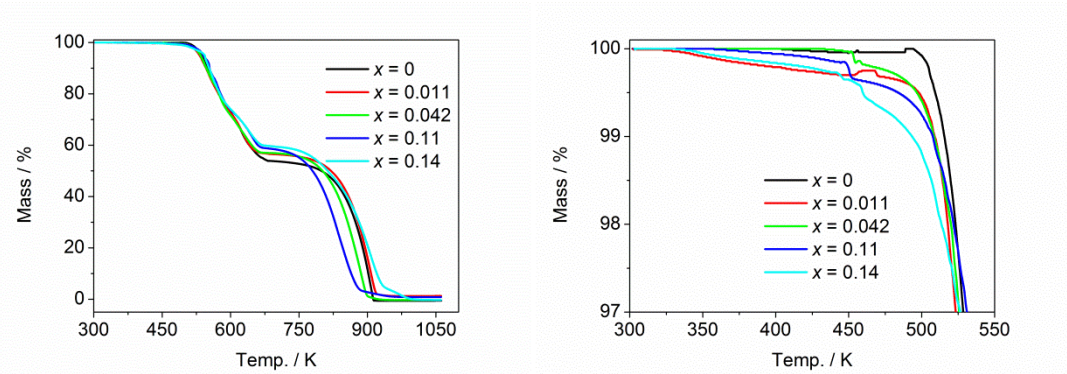

Fig. S8: TG plots of $Bu_4N_{1-x}Li_xMn_xPb_{1-x}I_3$ (x = 0–0.14).

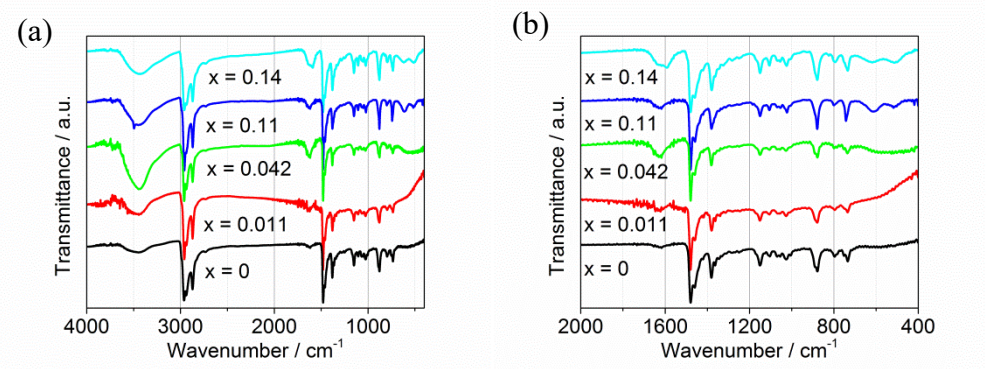

Fig. S9: IR spectra of $Bu_4N_{1-x}Li_xMn_xPb_{1-x}I_3$ (x = 0–0.14).

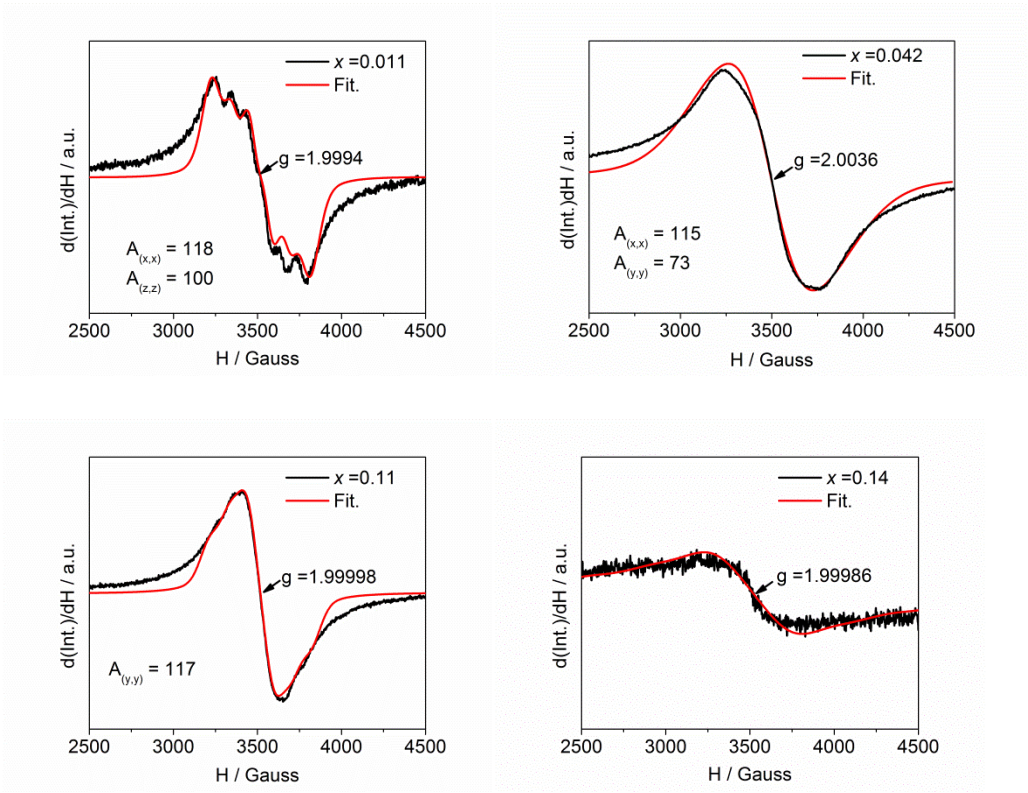

Fig. S10: Experimental and simulated EPR spectra of $Bu_4N_{1-x}Li_xMn_xPb_{1-x}I_3$ (x = 0.011–0.14) with g value ≈ 2.0 and average A value ~110 Gauss.

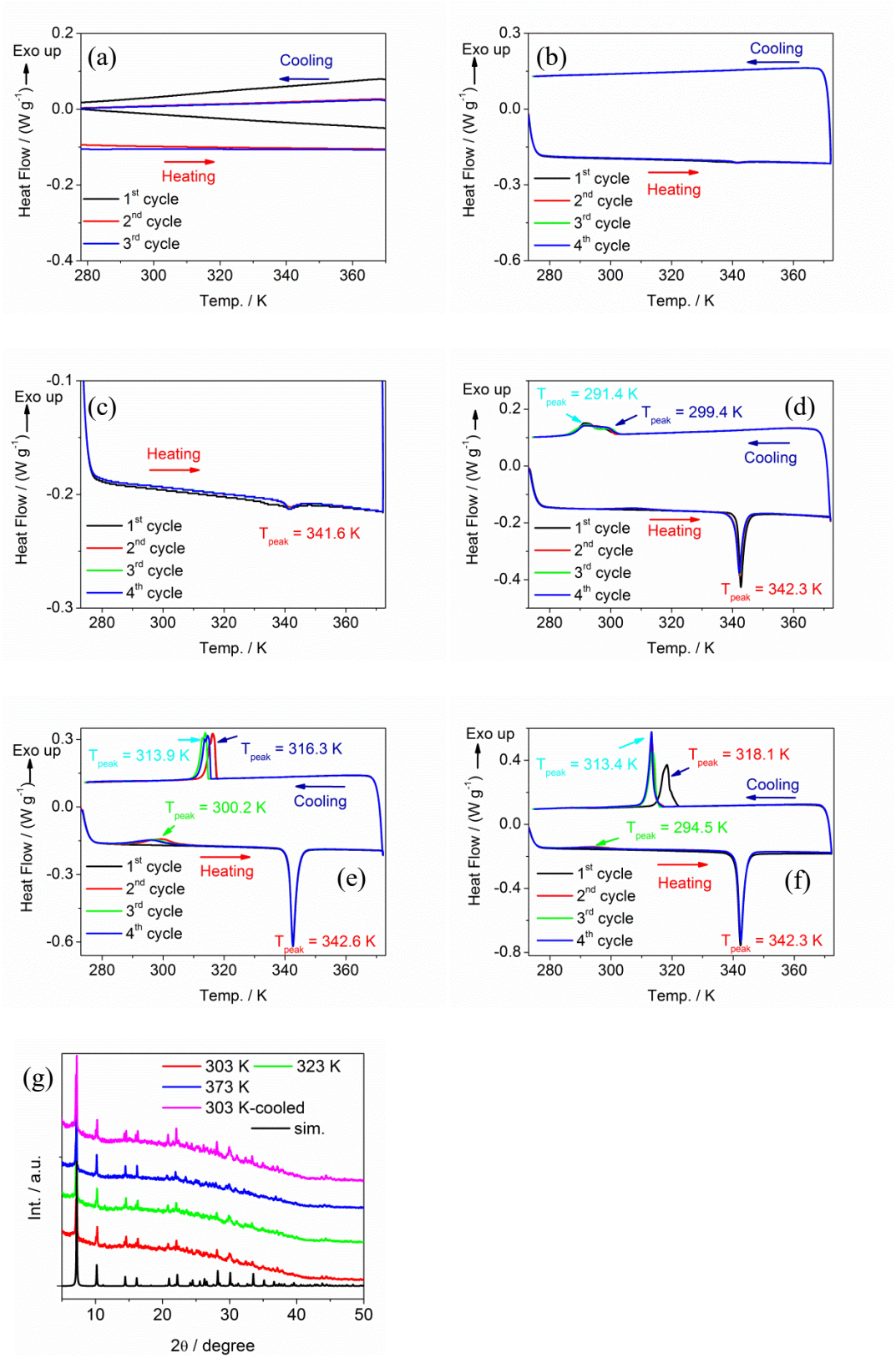

Fig. S11: DSC Plots of with x = (a) 0, (b, c) 0.011, (d) 0.042, (e) 0.11, (f) 0.14 with four heating and cooling cycles. (g) Variable-temperature PXRD patterns of $Bu_4N_{1-x}Li_xMn_xPb_{1-x}I_3$ with $x = 0.14$.

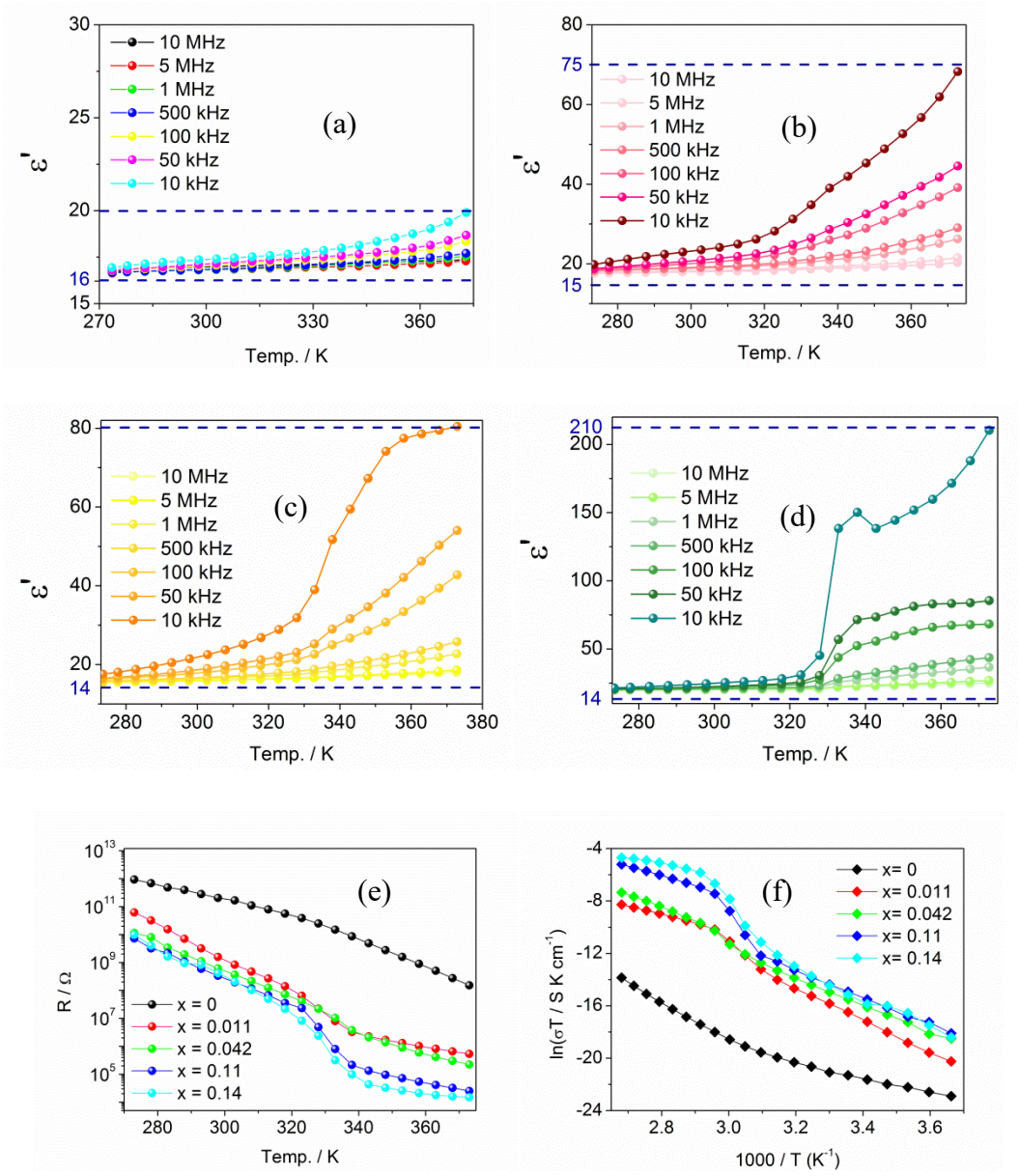

Fig. S12: Plots of dielectric permittivity *versus* temperature at the selected frequencies for $Bu_4N_{1-x}Li_xMn_xPb_{1-x}I_3$ with x = (a) 0, (b) 0.011, (c) 0.042 and (d) 0.11. (e) Resistance plots and (f) Arrhenius plots of $Bu_4N_{1-x}Li_xMn_xPb_{1-x}I_3$ (x = 0–0.14) at 273–373K.

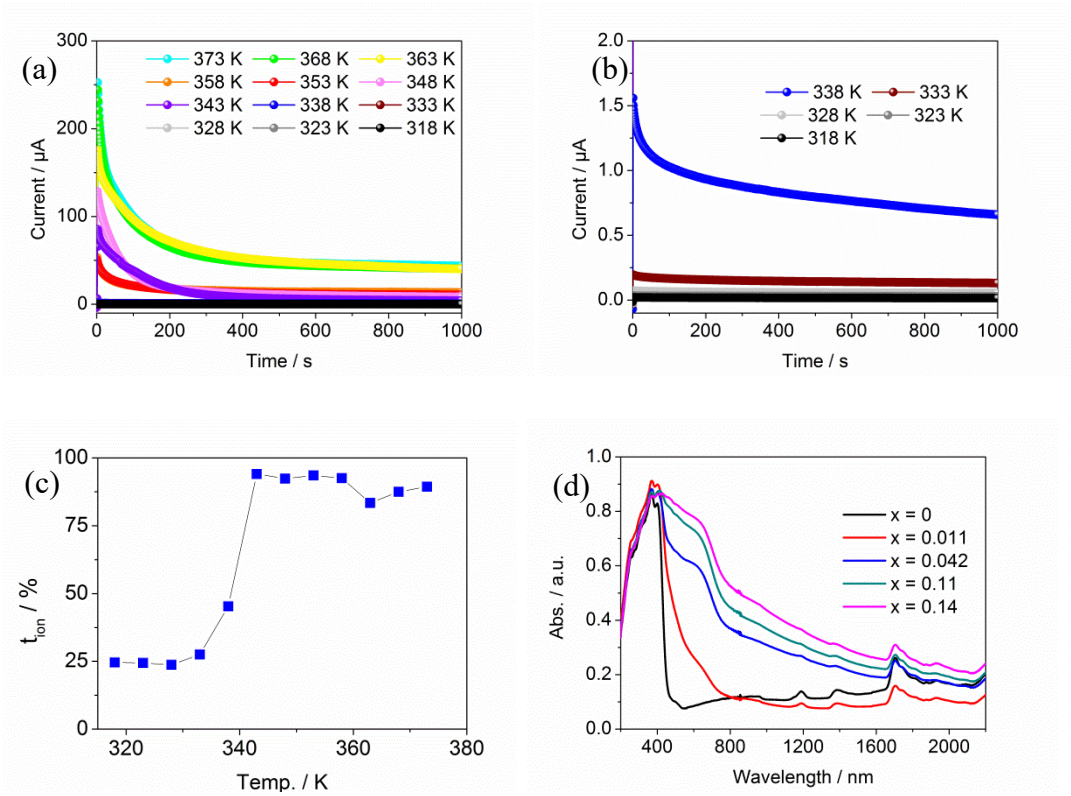

Fig. S13: Plots of (a, b) chronoamperometry of $Bu_4N_{1-x}Li_xMn_xPb_{1-x}I_3$ with x = 0–0.14. (c) Transference numbers of ion vs. temperature for $Bu_4N_{1-x}Li_xMn_xPb_{1-x}I_3$ with x = 0.14. (d) solid ultraviolet-visible near-IR spectra of $Bu_4N_{1-x}Li_xMn_xPb_{1-x}I_3$ with x = 0–0.14.

References

1. Y. J. She, S. P. Zhao, Z. F. Tian, X. M. Ren, *Inorg. Chem. Commun.* 2014, **46**, 29–32.
2. P. T. Zhang, K. Gaurav, H. Kengo, P. S. Shyam, T. L. Ma, H. Shuzi, *ACS Sustain. Chem. Eng*. 2018, **6**, 10221–10228.
3. S. G. Liu, P.J. Wu, Y. Q. Liu, D. B. Zhu, *Mol. Cryst. Liq. Cryst.*, 1997, **86**, 2265–2266.
4. A. Daniel, S. Sadasivan, A. A. David, A. A. Jouse, K. Bindu, *Sol. Energy.* 2019, **187**, 427–437.